

# Computational Studies of the Coordination Stereochemistry, Bonding, and Metal Selectivity of Mercury<sup>†</sup>

Hui-Chung Tai<sup>§</sup> and Carmay Lim<sup>\*.§.‡</sup>

Department of Chemistry, National Tsing Hua University, Hsinchu 300, Taiwan, and the Institute of Biomedical Sciences, Academia Sinica, Taipei 115, Taiwan

Received: June 5, 2005; In Final Form: September 19, 2005

Knowledge of the bonding and selectivity of organic mercury,  $[\text{H}_3\text{C}-\text{Hg}]^+$  ( $\text{MeHg}^+$ ), and inorganic  $\text{Hg}^{2+}$  for protein and DNA functional groups is important for understanding the mechanism of heavy metal poisoning. Herein, we elucidate (1) the differences between inorganic  $\text{Hg}^{2+}$  and organic  $\text{MeHg}^+$  in their interactions with different ligands of biological interest, (2) the protein and DNA functional groups that  $\text{Hg}^{2+}$  and  $\text{MeHg}^+$  target in aqueous solution, and (3) the likelihood of “soft”  $\text{Hg}^{2+}$  displacing the “borderline”  $\text{Zn}^{2+}$  bound to “harder” nitrogen/oxygen-containing side chains such as His and Asp/Glu. The results reveal that, relative to  $\text{Hg}^{2+}$ , the lower positive charge on  $\text{MeHg}^+$  results in a longer and weaker bond with a given ligand, in accord with the observed kinetic lability of  $\text{MeHg}^+$  complexes. They also indicate that negatively charged or polar amino acid side chains containing S<sup>-</sup>/O<sup>-</sup>/S/N donors could coordinate to both organic  $\text{MeHg}^+$  and inorganic  $\text{Hg}^{2+}$ . In addition, Gua and Cyt could also coordinate to  $\text{MeHg}^+$  and disrupt Gua···Cyt base pairing. A key novel finding is that  $\text{Hg}^{2+}$  is a far better electron acceptor than  $\text{Zn}^{2+}$ , and can thus accept more negative charge from the Zn ligands than the native  $\text{Zn}^{2+}$ , thus enhancing Hg–ligand interactions and enabling  $\text{Hg}^{2+}$  to displace the native cofactor from zinc essential enzymes and “structural” Zn proteins. The results herein support several possible mechanisms for Hg poisoning. Ways that mercury poisoning could be prevented in cells are discussed.

## Introduction

Elemental mercury (Hg), derived from the Greek word *hydrargyrios*, meaning “water silver”, is the only metal that is a silvery-white liquid at room temperature. Its unique liquid property stems from relativistic effects, resulting in a large 6s–6p energy gap, which limits effective hybrid orbital formation to linear sp, explaining the preponderance of linear Hg(II) compounds.<sup>1</sup> Partly for these reasons, the chemistry of mercury differs from that of zinc and cadmium (which belong to the same group in the periodic table) as well as that of other heavy metals. Apart from elemental Hg, mercury also exists in organic and inorganic (mercurous  $\text{Hg}^+$  and mercuric  $\text{Hg}^{2+}$ ) forms. Mercury in any form is toxic. Its toxic effects include irreversible damage to the nervous tissue and injury of the kidneys, liver, and lungs,<sup>2</sup> induction of autoimmune-like diseases,<sup>3–5</sup> and DNA cleavage.<sup>6–8</sup>

One likely cause of mercury’s acute toxicity to man stems from the high affinity of the “soft” (large, polarizable)  $\text{Hg}^{2+}$  for the “soft” donor sulfur,<sup>9</sup> which leads to toxic effects<sup>10</sup> in the following plausible ways. First,  $\text{Hg}^{2+}$  could promote the production of lipid peroxides, which alter membrane structure and disrupt mitochondrial function.<sup>11</sup> Second,  $\text{Hg}^{2+}$  could deplete the antioxidant peptide, glutathione (GSH), and inhibit the activities of enzymes involved in GSH metabolism (GSH synthetase and GSH reductase)<sup>12</sup> and free-radical quenching enzymes (catalase and superoxide dismutase),<sup>13</sup> thus inhibiting antioxidative processes. Third, the “soft”  $\text{Hg}^{2+}$  could displace the “borderline”<sup>9</sup> native  $\text{Zn}^{2+}$  cofactor from Cys-rich

binding sites such as Cys-rich metallothioneins<sup>14</sup> and Cys-rich Zn-finger cores and disrupt the critical function of these proteins.<sup>15–17</sup> This is supported by experiments showing that  $\text{Hg}^{2+}$  can dislodge  $\text{Zn}^{2+}$  from the Cys<sub>4</sub>-binding site of the DNA repair protein, Fpg, and a synthetic Cys<sub>2</sub>His<sub>2</sub> peptide.<sup>18,19</sup>

Another cause of mercury’s acute toxicity to man stems from the biological methylation of  $\text{Hg}^{2+}$  salts,<sup>10,20</sup> generating the methylmercury monocation,  $[\text{H}_3\text{C}-\text{Hg}]^+$  (denoted by  $\text{MeHg}^+$ ), one of the simplest and most harmful cationic species involved in the biogeochemical mercury cycle.<sup>1,21</sup> Several reasons have been proposed for the high toxicity of  $\text{MeHg}^+$  compounds. First, as for  $\text{Hg}^{2+}$ ,  $\text{MeHg}^+$  has high affinity for the “soft” donor sulfur; hence by binding to free sulfhydryl groups, it could disrupt the structure and function of essential proteins (see above). Second, it has high affinity for lipids, with a half-life in the human body of around 70 days, significantly longer than that of inorganic  $\text{Hg}^{2+}$  (4–5 days).<sup>1</sup> The strong tendency of  $\text{MeHg}^+$  to accumulate in the food chain makes it highly toxic to living organisms. Third,  $\text{MeHg}^+$  is highly mobile and has a low kinetic barrier for ligand exchange, i.e.,  $[\text{H}_3\text{C}-\text{Hg}-\text{L}_1] + \text{L}_2 \leftrightarrow [\text{H}_3\text{C}-\text{Hg}-\text{L}_2] + \text{L}_1$ ,<sup>1,22,23</sup> allowing it to form complexes in aqueous solution with a variety of ligands.

Although experimental and/or theoretical studies have been carried out on  $\text{MeHg}^+$  and  $\text{Hg}^{2+}$  complexes in aqueous solution,<sup>22,24–27</sup> the stability of the Hg–C bond,<sup>28–31</sup> and the interaction between  $\text{Hg}^{2+}$  and several biologically important groups,<sup>6,10,32–40</sup> no systematic theoretical studies have been carried out to address the following intriguing questions: (1) What are the differences between inorganic  $\text{Hg}^{2+}$  and organic  $\text{MeHg}^+$  in their interactions with different ligands? (2) Aside from the “soft” sulfur atom of Cys/Met and certain modified nucleosides, which other protein and DNA functional groups

<sup>†</sup> Part of the special issue “Donald G. Truhlar Festschrift”.

\* E-mail: carmay@gate.sinica.edu.tw.

§ National Tsing Hua University.

‡ Institute of Biomedical Sciences.

do  $\text{Hg}^{2+}$  and  $\text{MeHg}^+$  target in aqueous solution? (3) Can the “soft”  $\text{Hg}^{2+}$  compete with the “borderline”  $\text{Zn}^{2+}$  for the “harder” nitrogen/oxygen-containing side chains such as His and Asp/Glu, which are commonly found coordinated to  $\text{Zn}^{2+}$  in proteins where  $\text{Zn}^{2+}$  plays a predominantly catalytic role (“catalytic” Zn sites). To the best of our knowledge, no generic rules on  $\text{Zn}^{2+} \leftrightarrow \text{Hg}^{2+}$  in “catalytic” Zn sites have been reported.

Herein, we have carried out systematic theoretical studies on  $\text{Hg}^{2+}$  and  $\text{MeHg}^+$  interacting with various biological targets. Specifically, we have evaluated the structural and energetic features of organic  $[\text{H}_3\text{C}-\text{Hg}-\text{L}]^{1+z}$  and inorganic  $[\text{H}_2\text{O}-\text{Hg}-\text{L}]^{2+z}$  mercury complexes, which were designed to mimic linear structures observed in nature.<sup>1,9,34,38,39</sup> We considered ligands  $\text{L}^z$  ( $z = 0, -1$ ) modeling protein and DNA functional groups that could coordinate to the metal (Figure 1). The neutral ligands include  $\text{H}_2\text{O}$ ,  $\text{MeOH}$ ,  $\text{H}_2\text{S}$ ,  $\text{MeSH}$ ,  $\text{Me}_2\text{S}$ ,  $\text{NH}_3$ ,  $\text{MeNH}_2$ ,  $\text{NH}_2\text{-CH}_2\text{CONH}_2$  (Nbbk),  $\text{MeCONHMe}$  (Bkb), imidazole (Im), 9-methylpurine (MePur), 9-methyladenine (MeAde), 9-methylguanine (MeGua), and 1-methylcytosine MeCyt, while the negatively charged ligands include 1-methylthymidate ( $\text{MeThy}^-$ ), dimethyl phosphate ( $\text{DMP}^-$ ), acetate ( $\text{Ace}^-$ ),  $\text{MeS}^-$ , and  $\text{Cl}^-$ .

The differences between  $\text{Hg}^{2+}$  and  $\text{MeHg}^+$  in their interactions with different ligands were identified by comparing the molecular geometries and formation energies of linear  $[\text{H}_3\text{C}-\text{Hg}-\text{L}]^{1+z}$  and  $[\text{H}_2\text{O}-\text{Hg}-\text{L}]^{2+z}$  complexes and further decomposing the formation energy into the component interactions ( $\sigma$ - and  $\pi$ -type orbital interactions, electrostatic interactions, and Pauli repulsion). The protein and DNA functional groups targeted by  $\text{Hg}^{2+}$  and  $\text{MeHg}^+$  in aqueous solution were determined by computing the free energies for replacing water molecule(s) in hydrated  $\text{MeHg}^+$  or  $\text{Hg}^{2+}$  with model protein/DNA ligands. The possibility of  $\text{Hg}^{2+}$  displacing the native  $\text{Zn}^{2+}$  cofactor from “catalytic” Zn sites was evaluated by computing the free energies for replacing  $\text{Zn}^{2+}$  with  $\text{Hg}^{2+}$  in model rigid and flexible Zn-binding sites of varying degrees of solvent exposure.

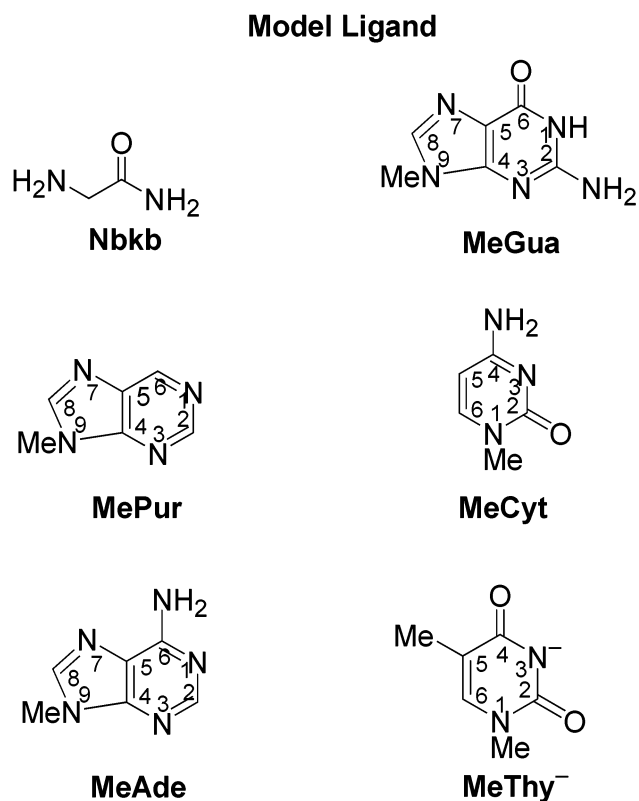
## Methods

**PDB Survey of Mercury Complexes.** The Protein Databank (PDB)<sup>41</sup> was surveyed for X-ray ( $<3.0 \text{ \AA}$  resolution) and NMR structures of proteins containing  $\text{Hg}^{2+}$ . Protein sequences with sequence identity higher than 30% were considered to belong to the same protein family. Only one representative from each protein family, namely, the structure solved at the highest resolution, was included. These structures are summarized in Table 1 in the Supporting Information.

**Geometry Optimization.** The geometries of  $\text{Hg}^{2+}$  and  $\text{MeHg}^+$  complexed with the ligands in Figure 1 as well as the geometries of  $\text{Zn}^{2+}$  and  $\text{Hg}^{2+}$  complexes in model Zn-binding sites were fully optimized using the *Gaussian 03* program,<sup>42</sup> with the B3-PW91 functional<sup>43,44</sup> in conjunction with the SDD basis set for mercury<sup>45</sup> and zinc,<sup>46</sup> and the 6-31+G(d)<sup>47-49</sup> basis set for the other atoms (referred to as basis set A). The B3-PW91/A method was also used to compute the vibrational frequencies of each fully optimized structure. No imaginary frequency was found in any of the molecules.

**Electronic Energy Calculations.** No gas-phase energies involving any of the Hg compounds studied here have been measured. Therefore, to assess if the B3-PW91/A method is also appropriate for computing electronic energies, we computed the gas-phase free energy for  $\text{CH}_3\text{Hg}^+ + \text{H}_2\text{O} \rightarrow [\text{H}_3\text{C}-\text{Hg}-\text{OH}_2]^+$  using both B3-PW91<sup>43,44</sup> and B3-LYP<sup>43,50</sup> functionals in combination with the SDD basis set for the metal and increasing basis sets for the other atoms. The results in Table 2

Model Ligand	Biological Relevance
$\text{H}_2\text{O}$	Solvent
$\text{MeOH}$	Ser side chain
$\text{H}_2\text{S}$	
$\text{MeSH}$	Cys side chain
$\text{Me}_2\text{S}$	Met side chain
$\text{NH}_3$	
$\text{MeNH}_2$	Deprotonated Lys side chain
Nbbk	N-terminal backbone
Bkb	Peptide backbone
Im	His side chain
MePur	
MeAde	Adenine base
MeGua	Guanine base
MeCyt	Cytosine base
$\text{MeThy}^-$	Deprotonated Thy base
$\text{Me}_2\text{PO}_4^-$	RNA/DNA phosphate
$\text{Ace}^-$	Asp side chain
$\text{MeS}^-$	Deprotonated Cys side chain
$\text{Cl}^-$	



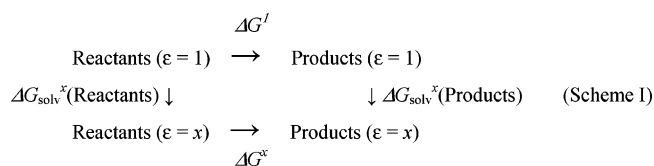
**Figure 1.** (a) Compounds (left) modeling protein and DNA functional groups (right) that could coordinate to mercury. (b) Stick drawings of the N-terminal backbone (Nbbk) and model DNA bases.

in the Supporting Information show that the gas-phase free energy computed using the B3-PW91/A method (−22.4 kcal/mol) is similar to that computed using B3-PW91 with the larger 6-311++G(2d,2p)<sup>47–49</sup> basis set (−22.1 kcal/mol), and is 1.1 kcal/mol more negative than the respective number computed using the B3-LYP functional. Furthermore, the magnitude of the formation energies of [H<sub>3</sub>C–Hg–L] (L = MeS<sup>−</sup>, Ace<sup>−</sup>, MeIm, Me<sub>2</sub>S) complexes computed using the B3-PW91/A method exhibit the same trend (MeS<sup>−</sup> > Ace<sup>−</sup> > MeIm > Me<sub>2</sub>S) as those computed using B3-LYP/6-311++G(2df,2pd)//B3-LYP/6-311+G(d) in previous work.<sup>35</sup> Thus, the B3-PW91/A method was used to evaluate the electronic energies of all the Hg<sup>2+</sup> and MeHg<sup>+</sup> complexes studied.

**Energy Decomposition of the Hg–L Bond.** To understand the nature of the Hg–L bond in the Hg<sup>2+</sup> and MeHg<sup>+</sup> complexes, the [H<sub>2</sub>O–Hg–L]<sup>2+z</sup> or [H<sub>3</sub>C–Hg–L]<sup>1+z</sup> formation energy was decomposed into orbital interaction energy, electrostatic energy, Pauli electron repulsion, and strain energy using Ziegler and Rauk's<sup>51,52</sup> energy decomposition scheme, as implemented in the Amsterdam Density Functional (ADF) 2000 program.<sup>53</sup> The further decomposition of the orbital interaction energy into the respective  $\sigma$  and  $\pi$  components requires a C<sub>s</sub>-symmetric Hg complex with an energy close to (within 3 kcal/mol) the energy of the fully optimized complex. Therefore, the [H<sub>3</sub>C–Hg–L]<sup>1+z</sup> and [H<sub>2</sub>O–Hg–L]<sup>2+z</sup> (z = 0, −1) complexes were reoptimized in C<sub>s</sub> symmetry. Because [H<sub>3</sub>C–Hg–L]<sup>+</sup> and [H<sub>2</sub>O–Hg–L]<sup>2+</sup> (L = MeOH and MeSH) have significantly less stable C<sub>s</sub> geometries (by more than 3 kcal/mol), as compared to the respective fully optimized geometries, energy decomposition analyses were not performed for these complexes.

Both C<sub>s</sub> geometry optimization and energy decomposition calculations were performed using the B-P86 functional<sup>54</sup> and a basis set combination, referred to as B, which employs uncontracted Slater-type orbitals as basis functions.<sup>55</sup> The valence basis functions have triple- $\zeta$  quality, augmented with two sets of p functions for Hg, Cl, P, and S, but with only one set of p functions for the other atoms. The (1s)<sup>2</sup> core electrons of C, N, O, and Na, the (1s2sp)<sup>10</sup> core electrons of P and S, and the (1s2sp3spd4spdf)<sup>60</sup> core electrons of Hg were treated within the frozen-core approximation.<sup>56</sup> Relativistic effects were treated by the zeroth-order regular approximation.<sup>57</sup> The geometries of the [H<sub>2</sub>O–Hg–L]<sup>2+z</sup> and [H<sub>3</sub>C–Hg–L]<sup>1+z</sup> (z = 0, −1) complexes were optimized using B-P86/B (rather than B3-PW91/A) for the energy decomposition analyses, because the SDD basis for Hg is not available in the ADF program. Furthermore, the B-P86/B method has been found to yield accurate Pt complex geometries.<sup>58</sup> It also yields fully optimized [H<sub>3</sub>C–Hg–L]<sup>1+z</sup> and [H<sub>2</sub>O–Hg–L]<sup>2+z</sup> (z = 0, −1) geometries that are similar to those produced by the B3-PW91/A method: the two methods yield C–Hg, O–Hg, and Hg–L bond distances as well as O–Hg–L and C–Hg–L of the [H<sub>3</sub>C–Hg–L]<sup>1+z</sup> and [H<sub>2</sub>O–Hg–L]<sup>2+z</sup> complexes that agree to within 0.02 Å and 3°, respectively.

**Free Energy Calculations.** The free energy for exchanging one ligand with another one in hydrated Hg<sup>2+</sup>/MeHg<sup>+</sup> or for replacing Zn<sup>2+</sup> with Hg<sup>2+</sup> in model Zn-binding sites in an environment characterized by a dielectric constant  $\epsilon = x$  was calculated using Scheme 1



where  $\Delta G^x$  is given by

$$\Delta G^x = \Delta G^1 + \Delta G_{\text{solv}}^x(\text{Products}) - \Delta G_{\text{solv}}^x(\text{Reactants}) \quad (1)$$

The gas-phase free energy,  $\Delta G^1$ , at room temperature,  $T = 298.15$  K, was computed according to

$$\Delta G^1 = \Delta E_{\text{elec}} + \Delta E_{\text{T}} + \Delta PV - T\Delta S \quad (2)$$

where  $\Delta$  denotes the difference between the product(s) and reactant(s), while  $E_{\text{elec}}$ ,  $E_{\text{T}}$ ,  $PV$ , and  $S$  are, respectively, the electronic energy, thermal energy, work term, and total entropy. The geometries and electronic energies were evaluated at the B3-PW91/A level, while the vibrational energies and entropies were derived from the B3-PW91/A frequencies scaled by an empirical factor of 0.9573.<sup>59</sup>

The electrostatic contribution to the solvation free energy,  $\Delta G_{\text{solv}}^x$ , is the difference between the free energies of charging the molecule in vacuo ( $\epsilon = 1$ ) and in a given dielectric medium ( $\epsilon = x$ ), which, in turn, can be derived from the difference between the electrostatic potential in  $\epsilon = x$  and that in  $\epsilon = 1$ . The electrostatic potentials were obtained by numerical solution of the Poisson–Boltzmann equation using the Jaguar 5.5 program.<sup>60</sup> On the basis of the fully optimized B3-PW91/A geometries, the  $\Delta G_{\text{solv}}^x$  values were computed using the B3-LYP functional in combination with the LACV3P\*\* basis set for the metal and the cc-pVTZ(-f)++ basis set for the other atoms,<sup>60</sup> as well as default dielectric radii in Jaguar and effective radii optimized in this work (see below).

The default dielectric radii in Jaguar have been optimized to reproduce experimental hydration free energies and pK<sub>a</sub> in conjunction with the B3-LYP functional and the cc-pVTZ(-f)++ basis set for nonmetal atoms. With these radii, the computed  $\Delta G_{\text{solv}}^x$  for the ligands in Figure 1 (except Nbbk, MePur, MeGua, MeCyt, and MeThy<sup>−</sup>, for which experimental hydration free energies could not be found) are within 1.5 kcal/mol of the respective experimental values (Table 3 in the Supporting Information).

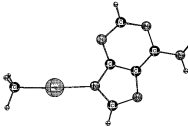
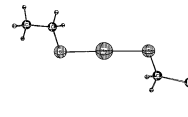

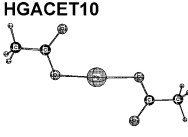
Effective radii for [Zn (H<sub>2</sub>O)<sub>6</sub>]<sup>2+</sup>, [Hg (H<sub>2</sub>O)<sub>6</sub>]<sup>2+</sup>, and [H<sub>3</sub>C–Hg–OH<sub>2</sub>]<sup>+</sup> have not been parametrized in Jaguar. For hexahydrated Zn<sup>2+</sup> and Hg<sup>2+</sup>, the metal (M) and respective water (W) oxygen and hydrogen radii were simultaneously adjusted to reproduce the “experimental” hydration free energy of [M W<sub>6</sub>]<sup>2+</sup>, which was estimated from the measured hydration free energy,  $\Delta G_{\text{solv,expt}}^{80}(\text{M}^{2+})$  and the computed gas-phase free energy,  $\Delta G_{\text{calc}}^1$ , for  $\text{M}^{2+} + 6\text{W} \rightarrow [\text{M W}_6]^{2+}$ ; that is

$$\Delta G_{\text{solv,expt}}^{80}([\text{M W}_6]^{2+}) \approx \Delta G_{\text{solv,expt}}^{80}(\text{M}^{2+}) - \Delta G_{\text{calc}}^1(\text{M}^{2+} + 6\text{W} \rightarrow [\text{M W}_6]^{2+}) \quad (3)$$

In computing  $\Delta G_{\text{calc}}^1$ , a counterpoise correction was applied to the gas-phase energy,  $\Delta E_{\text{elec}}$ , because basis set superposition error may be significant in complex formation reactions. The resulting optimized radii ( $R_{\text{Zn}} = 1.38$  Å,  $R_{\text{Hg}} = 2.10$  Å,  $R_{\text{O}} = 1.55$  Å,  $R_{\text{H}} = 1.07$  Å) yield  $\Delta G_{\text{solv}}^{80}$  that are within ~1% of the absolute “experimental” hydration free energies of hexahydrated Zn<sup>2+</sup> and Hg<sup>2+</sup> (Table 3 in Supporting Information). On the other hand, effective radii for the Hg, C, and H atoms of MeHg<sup>+</sup> were obtained by adjusting them to reproduce available experimental data involving MeHg<sup>+</sup>. The resulting optimized radii ( $R_{\text{Hg}(\text{MeHg})} = 2.10$  Å,  $R_{\text{C}(\text{MeHg})} = 1.63$  Å,  $R_{\text{H}(\text{MeHg})} = 0.48$  Å) yield  $\Delta G_{\text{calc}}^{80}$  that are close to the experimental  $\Delta G_{\text{expt}}^{80}$  (Table 4 in Supporting Information).



**TABLE 1: Comparison between Calculated and Experimental Bond Distances (in Å) and Angles (in deg) for Hg Complexes**

		B3-LYP	B-P86	S-VWN	B3-PW91	Experiment
<b>ADMEHH</b> 	Hg-C	2.089	2.085	2.034	2.071	2.055
	Hg-N	2.095	2.095	2.044	2.078	2.071
	C-Hg-N	179.7	179.6	179.1	179.7	176.8
<b>MERSET01</b> 	Hg-S	2.379	2.375	2.317	2.356	2.343
	S-C	1.861	1.867	1.832	1.848	1.833
	S-Hg-S	178.0	177.9	178.6	178.0	176.5
	Hg-S-C	103.3	103.1	102.3	103.2	104.4
<b>H<sub>3</sub>C-Hg-Cl</b> 	Hg-C	2.101	2.096	2.043	2.082	2.061
	Hg-Cl	2.362	2.357	2.300	2.340	2.282
	C-Hg-Cl	180.0	180.0	180.0	180.0	180.0
<b>HGACET10</b> 	Hg-O	2.089	2.126	2.083	2.077	2.079
	O-Hg-O	173.2	171.0	169.2	172.8	176.0
	Rmsd (Å)	0.041	0.043	0.019	0.025	
	Rmsd (°)	2.0	2.7	3.5	2.1	

## Results

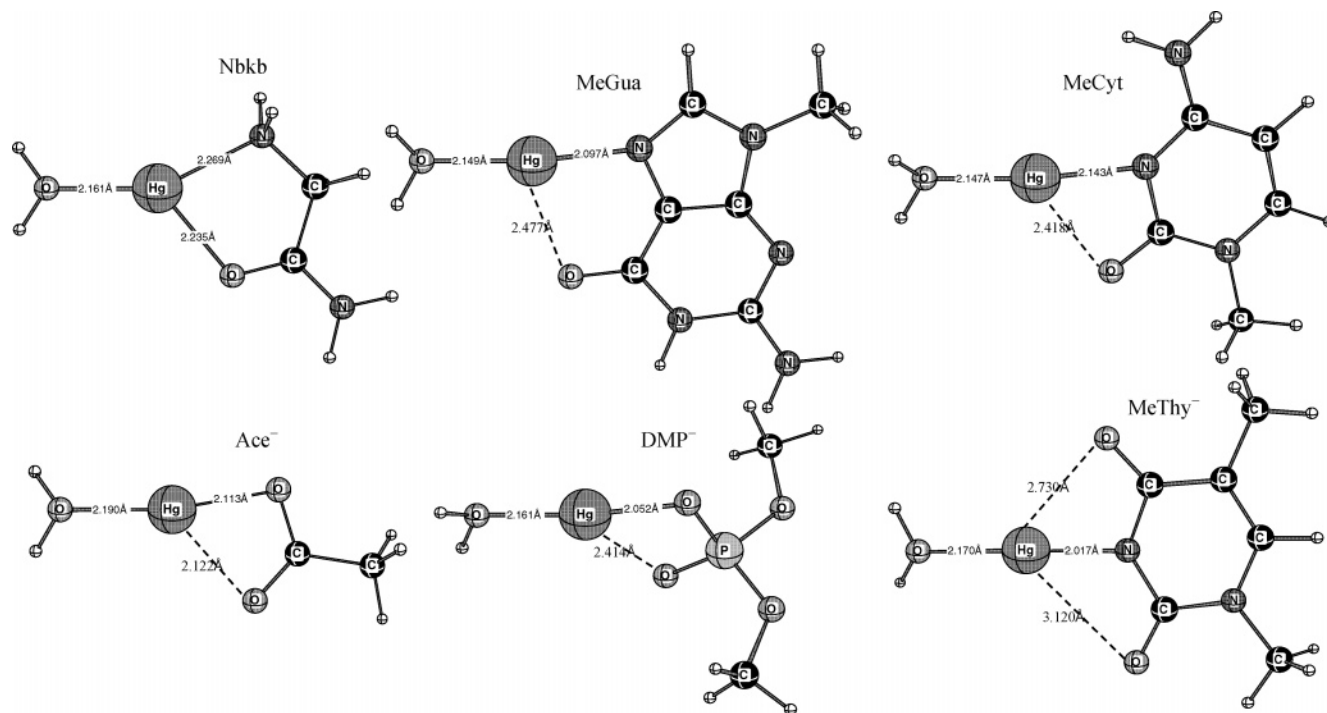
**Comparison Between Computed and Experimental Hg<sup>2+</sup> and MeHg<sup>+</sup> Complex Structures.** The Cambridge Structure Database<sup>61</sup> (CSD) was searched for X-ray structures of Hg<sup>2+</sup> bound to both neutral and negatively charged ligands containing C-, N-, O-, and S-donor atoms that can be used to calibrate the predicted geometries. This resulted in three pertinent CSD structures with *R*-factors of <10% (CSD codes ADMEHH, HGACET10, and MERSET01). In addition to the CSD structures, the structure of one of the complexes studied, [H<sub>3</sub>C-Hg-Cl]<sup>0</sup>, has been determined from pure rotational spectra<sup>62</sup> and was also used for geometry calibration. The aforementioned experimental structures were fully optimized using the *Gaussian 03* program<sup>42</sup> with the B3-LYP,<sup>43,50</sup> B-P86,<sup>54</sup> S-VWN,<sup>63</sup> and B3-PW91<sup>43,44</sup> functionals in combination with the SDD basis set for the metal<sup>45</sup> and the 6-31+G(d)<sup>47-49</sup> basis set for the other atoms (referred to as basis set A). Comparison of the fully optimized structures with the respective X-ray structures in Table 1 shows that, among the various methods, the B3-PW91 functional yielded both bond distances and angles in closest agreement with the corresponding experimental values with a root-mean-square deviation (RMSD) of 0.025 Å and 2.1°. Although the S-VWN functional yielded the least RMSD (0.019 Å) from the experimental bond distances, it also yielded the largest RMSD (3.5°) from the experimental bond angles.

**Comparison Between Linear Hg<sup>2+</sup> and MeHg<sup>+</sup> Complex Structures.** Comparison of the computed bond angles and distances in linear Hg<sup>2+</sup> and MeHg<sup>+</sup> complexes in Table 2 reveal interesting trends that could be rationalized by the charge difference between Hg<sup>2+</sup> and MeHg<sup>+</sup>. Hg(II) is expected to interact more strongly with a negatively charged methyl anion than with a neutral water molecule; hence, the C-Hg(L) bond length is generally shorter than the corresponding O-Hg(L) distance (Table 2). As compared to MeHg<sup>+</sup>, the greater positive charge on Hg<sup>2+</sup> results in a shorter Hg-L bond length (by 0.04 to 0.19 Å) and less linear structures (Table 2, O-Hg-L < C-MeHg-L). If the ligand L contains two donor atoms, X and Y, near each other, Hg<sup>2+</sup> not only coordinates with X, but also

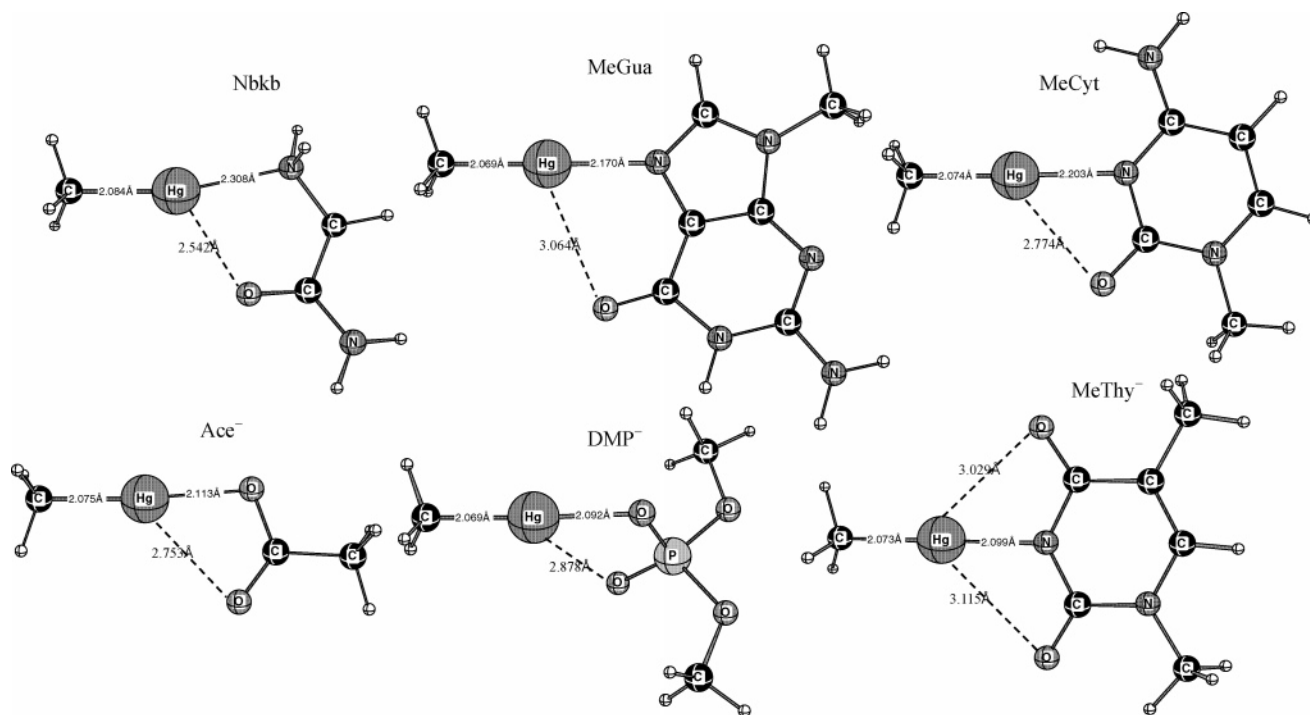
**TABLE 2: Calculated Bond Distances (in Å), Bond Angles (in deg), and Formation Energies (ΔE in kcal/mol) of Linear [H<sub>3</sub>C-Hg-L]<sup>1+</sup> and [H<sub>2</sub>O-Hg-L]<sup>2+</sup> Complexes<sup>a</sup>**

L	H <sub>2</sub> O	MeOH	H <sub>2</sub> S	MeSH	Me <sub>2</sub> S	NH <sub>3</sub>	MeNH <sub>2</sub>	Nbkb	Im	MePur	MeAde	MeGua	MeCyt	MeThy <sup>-</sup>	DMP <sup>-</sup>	Ace <sup>-</sup>	MeS <sup>-</sup>	Cl <sup>-</sup>
r(O-Hg) <sup>b</sup>	2.08	2.09	2.12	2.13	2.15	2.09	2.11	2.16	2.10	2.12	2.17	2.15	2.15	2.17	2.16	2.19	2.23	2.16
r(C-Hg) <sup>c</sup>	2.08	2.08	2.09	2.09	2.09	2.07	2.07	2.08	2.07	2.07	2.07	2.07	2.07	2.07	2.07	2.08	2.10	2.08
r(Hg-L) <sup>d</sup>	2.08	2.06	2.41	2.41	2.41	2.10	2.10	2.24	2.02	2.03	2.11	2.10	2.14	2.02	2.05	2.11	2.32	2.25
r(MeHg-L) <sup>e</sup>	2.25	2.22	2.57	2.54	2.52	2.23	2.22	2.31	2.16	2.16	2.15	2.17	2.20	2.10	2.09	2.11	2.38	2.34
O-Hg-L	177	176	176	176	175	178	178	130	177	177	164	173	174	179	172	170	175	178
C-Hg-L	178	179	179	178	178	180	180	168	180	180	180	179	179	180	176	175	178	180
CT <sup>f</sup>	0.21	0.28	0.53	0.61	0.67	0.37	0.43	0.41	0.40	0.45	0.41	0.40	0.43	0.57	0.44	0.55	0.90	0.64
CT <sup>g</sup>	0.10	0.12	0.25	0.28	0.31	0.19	0.21	0.20	0.20	0.20	0.21	0.20	0.48	0.54	0.21	0.28	0.49	0.36
ΔE <sup>h</sup>	-83	-97	-106	-124	-139	-121	-132	-165	-152	-144	-155	-182	-172	-362	-334	-353	-388	-345
ΔE <sup>i</sup>	-33	-36	-35	-42	-47	-52	-55	-61	-64	-51	-50	-67	-64	-170	-154	-171	-189	-170

<sup>a</sup> Fully optimized structures and energies are computed at the B3-PW91/A level (see Methods). <sup>b</sup> O(water)-Hg = 2.140 Å in the free state (no L). <sup>c</sup> C(Me)-Hg = 2.162 Å in the free state (no L). <sup>d</sup> Hg-L bond distance in inorganic [H<sub>2</sub>O-Hg-L]<sup>2+</sup> complexes. <sup>e</sup> Hg-L bond distance in organic [H<sub>3</sub>C-Hg-L]<sup>1+</sup> complexes. <sup>f</sup> Net NBO charge transferred by the ligand L to Hg in inorganic [H<sub>2</sub>O-Hg-L]<sup>2+</sup> complexes. <sup>g</sup> Net NBO charge transferred by the ligand L to Hg in organic [H<sub>3</sub>C-Hg-L]<sup>1+</sup> complexes. <sup>h</sup> Formation energy of [H<sub>2</sub>O-Hg-L]<sup>2+</sup> + L<sup>-</sup> → [H<sub>2</sub>O-Hg-L]<sup>2+</sup>. <sup>i</sup> Formation energy of [H<sub>3</sub>C-Hg-L]<sup>1+</sup> + L<sup>-</sup> → [H<sub>3</sub>C-Hg-L]<sup>1+</sup>.



**Figure 2.** Fully optimized B3-PW91/A structures of linear inorganic mercury complexes,  $[\text{H}_2\text{O}-\text{Hg}-\text{L}]^{2+z}$ , with  $\text{L} = \text{Nbbk}$ ,  $\text{MeGua}$ ,  $\text{MeCyt}$ ,  $\text{Ace}^-$ ,  $\text{DMP}^-$ , and  $\text{MeThy}^-$ .



**Figure 3.** Fully optimized B3-PW91/A structures of linear organic mercury complexes,  $[\text{H}_3\text{C}-\text{Hg}-\text{L}]^{1+z}$ , with  $\text{L} = \text{Nbbk}$ ,  $\text{MeGua}$ ,  $\text{MeCyt}$ ,  $\text{Ace}^-$ ,  $\text{DMP}^-$ , and  $\text{MeThy}^-$ .

attracts the nearby Y. For  $\text{L} = \text{Nbbk}$ ,  $\text{Hg}^{2+}$  coordinates bidentately to both the amide nitrogen and carbonyl oxygen atoms (Figure 2,  $r(\text{Hg}-\text{N}) - r(\text{Hg}-\text{O}) = 0.03 \text{ \AA}$ ); hence, the  $[\text{H}_2\text{O}-\text{Hg}-\text{Nbbk}]^{2+}$  structure is significantly bent with an  $\text{O}-\text{Hg}-\text{N}$  angle of  $130^\circ$ , whereas  $\text{MeHg}^+$  coordinates monodentately to the amide group (Figure 3,  $r(\text{MeHg}-\text{O}) - r(\text{MeHg}-\text{N}) = 0.23 \text{ \AA}$ ). Likewise,  $\text{Hg}^{2+}$  coordinates bidentately to both acetate oxygen atoms, whereas  $\text{MeHg}^+$  coordinates

monodentately, resulting in similar metal–O(Ace) distances. In contrast to  $\text{Nbbk}$  and  $\text{Ace}^-$ , both  $\text{Hg}^{2+}$  and  $\text{MeHg}^+$  coordinate monodentately to dimethyl phosphate and to the Bkb oxygen (rather than the Bkb nitrogen), in accord with the PDB structures.

**Similarities Among Stabilization Energy Trends of  $\text{Hg}^{2+}$  and  $\text{MeHg}^+$  Complexes.** Among all the ligands studied,  $\text{MeS}^-$  forms the strongest bond with both  $\text{Hg}^{2+}$  ( $-388 \text{ kcal/mol}$ ) and

**TABLE 3: Energy Decomposition of the Hg–L Bond in the  $C_s$ -Symmetric Linear  $[\text{H}_2\text{O}-\text{Hg}-\text{L}]^{2+z}$  and  $[\text{H}_3\text{C}-\text{Hg}-\text{L}]^{1+z}$  Complexes**

	H <sub>2</sub> O	H <sub>2</sub> S	Me <sub>2</sub> S	NH <sub>3</sub>	MeNH <sub>2</sub>	Nbkb	MeIm	MePur	MeAde	MeGua	DMP <sup>-</sup>	Ace <sup>-</sup>	MeS <sup>-</sup>	Cl <sup>-</sup>
$\Delta E_{C_s}$	-83.0	-96.6	-134.5	-121.5	-135.1	-169.2	-165.1	-155.5	-155.7	-174.2	-342.2	-363.2	-398.7	-359.4
$\Delta E'_{C_s}$	-31.7	-36.4	-50.8	-49.9	-54.4	-60.9	-66.4	-56.4	-56.1	-72.5	-153.9	-174.7	-193.4	-179.2
$\Delta E_{\text{str}}$	1.2	16.2	18.1	1.1	2.8	9.3	5.1	5.8	7.8	18.7	26.6	5.1	3.9	0.5
$\Delta E'_{\text{str}}$	1.0	1.1	2.3	1.6	2.3	8.0	3.5	3.9	4.7	5.3	13.6	6.3	3.5	2.5
$\Delta E_{\text{str}}(\text{L})$	0.6	15.7	17.4	0.4	2.2	8.6	4.4	5.1	7.1	18.1	26.2	4.2	2.1	0.0
$\Delta E'_{\text{str}}(\text{L})$	0.1	0.1	0.9	0.1	0.7	6.5	1.4	1.9	2.7	3.3	11.3	3.8	0.7	0.0
$\Delta E_{\text{str}}(\text{Hg}^{2+})$	0.6	0.5	0.7	0.7	0.6	0.7	0.7	0.7	0.7	0.6	0.4	0.9	1.8	0.5
$\Delta E'_{\text{str}}(\text{MeHg}^+)$	0.9	1.0	1.4	1.5	1.6	1.5	2.1	2.0	2.0	2.0	2.3	2.5	2.8	2.5
$\Delta E_{\text{int}}$	-84.2	-112.8	-152.6	-122.6	-137.9	-178.5	-170.2	-161.3	-163.5	-192.9	-368.8	-368.3	-402.6	-359.9
$\Delta E'_{\text{int}}$	-32.7	-37.5	-53.1	-51.5	-56.7	-68.9	-69.9	-60.3	-60.8	-77.8	-167.5	-181.0	-196.9	-181.7
$\Delta E_{\text{Pauli}}$	63.6	76.2	85.3	99.4	101.2	91.7	128.6	99.6	105.3	95.1	119.7	94.7	161.9	134.9
$\Delta E'_{\text{Pauli}}$	43.3	63.3	80.7	79.4	85.6	80.0	101.1	95.6	102.7	92.0	95.0	102.1	159.5	114.6
$\Delta E_{\text{elec}}$	-79.9	-77.8	-99.7	-128.5	-133.2	-146.4	-170.2	-127.8	-129.2	-150.7	-342.5	-325.2	-381.6	-351.1
$\Delta E'_{\text{elec}}$	-47.6	-54.0	-75.0	-85.1	-91.9	-93.8	-110.4	-95.9	-99.5	-107.5	-189.5	-206.2	-256.0	-214.2
$\Delta E_{\text{orb}}$	-67.9	-111.2	-138.1	-93.4	-105.9	-123.8	-128.6	-133.1	-139.6	-137.3	-146.0	-137.8	-182.8	-143.7
$\Delta E'_{\text{orb}}$	-28.4	-46.8	-58.7	-45.7	-50.4	-55.1	-60.5	-59.9	-64.0	-62.3	-73.0	-76.9	-100.4	-82.1
$\Delta E_{\text{orb}}(\text{a}')$	-61.3	-104.3	-125.5	-85.4	-96.7	-104.7	-99.4	-105.2	-110.8	-104.5	-123.4	-123.1	-161.2	-127.9
$\Delta E'_{\text{orb}}(\text{a}')$	-26.3	-44.0	-53.6	-42.7	-46.8	-49.3	-50.2	-48.5	-52.0	-50.4	-63.6	-68.5	-88.6	-73.9
$\Delta E_{\text{orb}}(\text{a}'')$	-6.6	-6.9	-12.7	-8.0	-9.2	-19.1	-29.2	-27.8	-28.8	-32.8	-22.6	-14.7	-21.6	-15.8
$\Delta E'_{\text{orb}}(\text{a}'')$	-2.1	-2.8	-5.2	-3.1	-3.6	-5.8	-10.3	-11.4	-12.1	-11.8	-9.4	-8.4	-11.8	-8.2

MeHg<sup>+</sup> (-189 kcal/mol). Among the neutral ligands, NH<sub>3</sub> or MeNH<sub>2</sub> form a stronger bond with both metal ions than SH<sub>2</sub> or MeSH, respectively, while among the model neutral DNA bases, MeGua and MeCyt form a stronger bond with both Hg<sup>2+</sup> and MeHg<sup>+</sup> than MeAde or MePur (Table 2,  $|\Delta E(\text{MeGua}/\text{MeCyt})| > |\Delta E(\text{MeAde}/\text{MePur})|$ ). The latter is probably because of favorable electrostatic interactions between the metal ion and the carbonyl oxygen in MeGua and MeCyt (Figures 2 and 3), which are absent in MeAde and MePur (Figure 1b). Replacing a ligand's hydrogen atom with a methyl group leads to additional stabilization of the Hg–L bond (Table 2, compare  $\Delta E/\Delta E'$  of  $H-\text{OH}$  and  $H_3\text{C}-\text{OH}$ ,  $H-\text{SH}$  and  $H_3\text{C}-\text{SH}$ ,  $H_3\text{C}-\text{S}-H$  and  $H_3\text{C}-\text{S}-\text{CH}_3$ ,  $H-\text{NH}_2$  and  $H_3\text{C}-\text{NH}_2$ ).

**Differences Between Stabilization Energy Trends of Hg<sup>2+</sup> and MeHg<sup>+</sup> Complexes.** Relative to the linear MeHg<sup>+</sup> complexes, the generally shorter Hg–L bond in the Hg<sup>2+</sup> counterparts correlates with the more favorable  $[\text{H}_2\text{O}-\text{Hg}-\text{L}]^{2+z}$  formation energies. Replacing an H atom with a methyl group stabilizes the Hg–L bond in  $[\text{H}_2\text{O}-\text{Hg}-\text{L}]^{2+z}$  (by 11–18 kcal/mol) more than the Hg–L bond in  $[\text{H}_3\text{C}-\text{Hg}-\text{L}]^{1+z}$  (by 3–7 kcal/mol) (L = H<sub>2</sub>O, NH<sub>3</sub>, H<sub>2</sub>S, and MeSH). These differences between linear Hg<sup>2+</sup> and MeHg<sup>+</sup> complexes may be rationalized in terms of the lower positive charge on MeHg<sup>+</sup> and, hence, less charge transfer from a given L to MeHg<sup>+</sup>, as compared to Hg<sup>2+</sup> (Table 2, CT' < CT).

**Energy Decomposition of the Hg–L Bond.** To understand the nature of the Hg–L bond in the Hg<sup>2+</sup> and MeHg<sup>+</sup> complexes, the Hg–L bond formation energy,  $\Delta E_{C_s}$ , of the  $C_s$ -symmetric complexes was decomposed into contributions from the strain energy,  $\Delta E_{\text{str}}$ , and the interaction energy,  $\Delta E_{\text{int}}$ ; i.e.,  $\Delta E_{C_s} = \Delta E_{\text{str}} + \Delta E_{\text{int}}$ . The latter can be further divided into three components: (1) the repulsion between the ligand and metal fragments according to the Pauli principle,  $\Delta E_{\text{Pauli}}$ , (2) the electrostatic interaction between the two,  $\Delta E_{\text{elec}}$ , and (3) the stabilizing orbital interactions,  $\Delta E_{\text{orb}}$ ; i.e.,  $\Delta E_{\text{int}} = \Delta E_{\text{Pauli}} + \Delta E_{\text{elec}} + \Delta E_{\text{orb}}$ . The energy components of the  $C_s$ -symmetric linear  $[\text{H}_2\text{O}-\text{Hg}-\text{L}]^{2+z}$  and  $[\text{H}_3\text{C}-\text{Hg}-\text{L}]^{1+z}$  complexes are listed in Table 3.

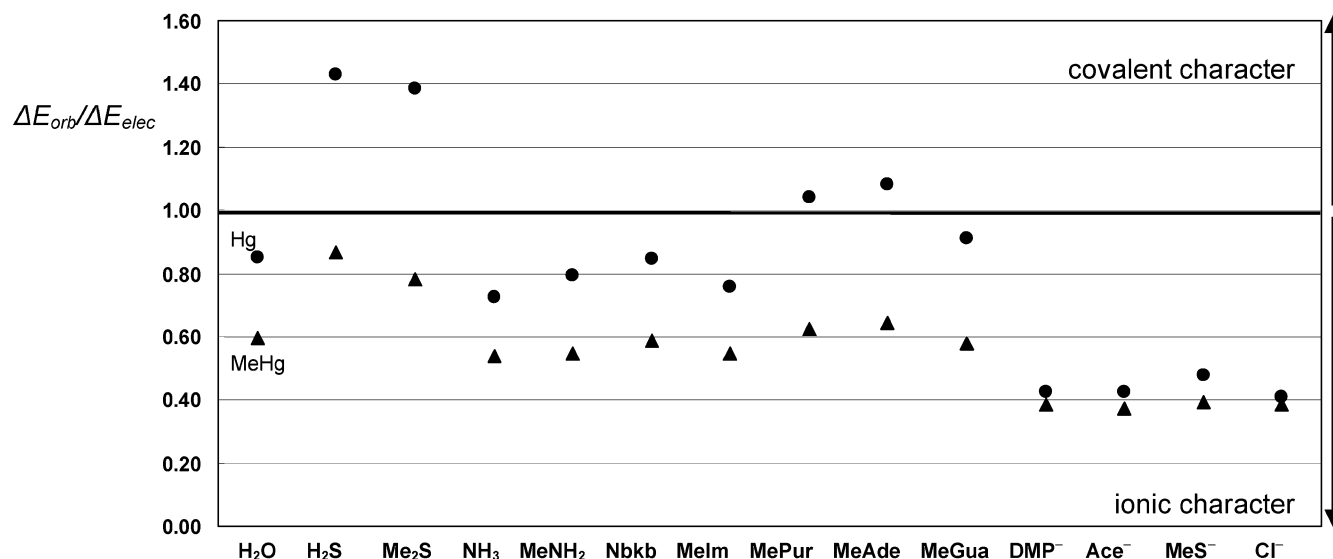
The interaction energy,  $\Delta E_{\text{int}}$ , between the distorted ligand L and the distorted  $[\text{H}_3\text{C}-\text{Hg}]^+$  or  $[\text{H}_2\text{O}-\text{Hg}]^{2+}$  fragments, rather than the energy,  $\Delta E_{\text{str}}$ , associated with deforming the equilibrium structures of the metal fragment and the free ligand

toward their respective geometry in the  $[\text{H}_3\text{C}-\text{Hg}-\text{L}]^{1+z}$  and  $[\text{H}_2\text{O}-\text{Hg}-\text{L}]^{2+z}$  complexes, dictates the net Hg–L bond formation energy (Table 3). In general, the favorable electrostatic interactions,  $\Delta E_{\text{elec}}$ , alone can generally offset the unfavorable Pauli repulsion,  $\Delta E_{\text{Pauli}}$ . They provide a larger stabilizing contribution than the orbital interactions,  $\Delta E_{\text{orb}}$  (except Hg<sup>2+</sup> ligated with H<sub>2</sub>S, Me<sub>2</sub>S, MePur, and MeAde), which are dictated by  $\sigma$  interactions,  $\Delta E_{\text{orb}}(\text{a}')$ , rather than by  $\pi$  interactions,  $\Delta E_{\text{orb}}(\text{a}'')$ . However, the complexes of the N-ring ligands show greater contribution of  $\pi$  interactions in forming the Hg–L bond than the other neutral ligands.

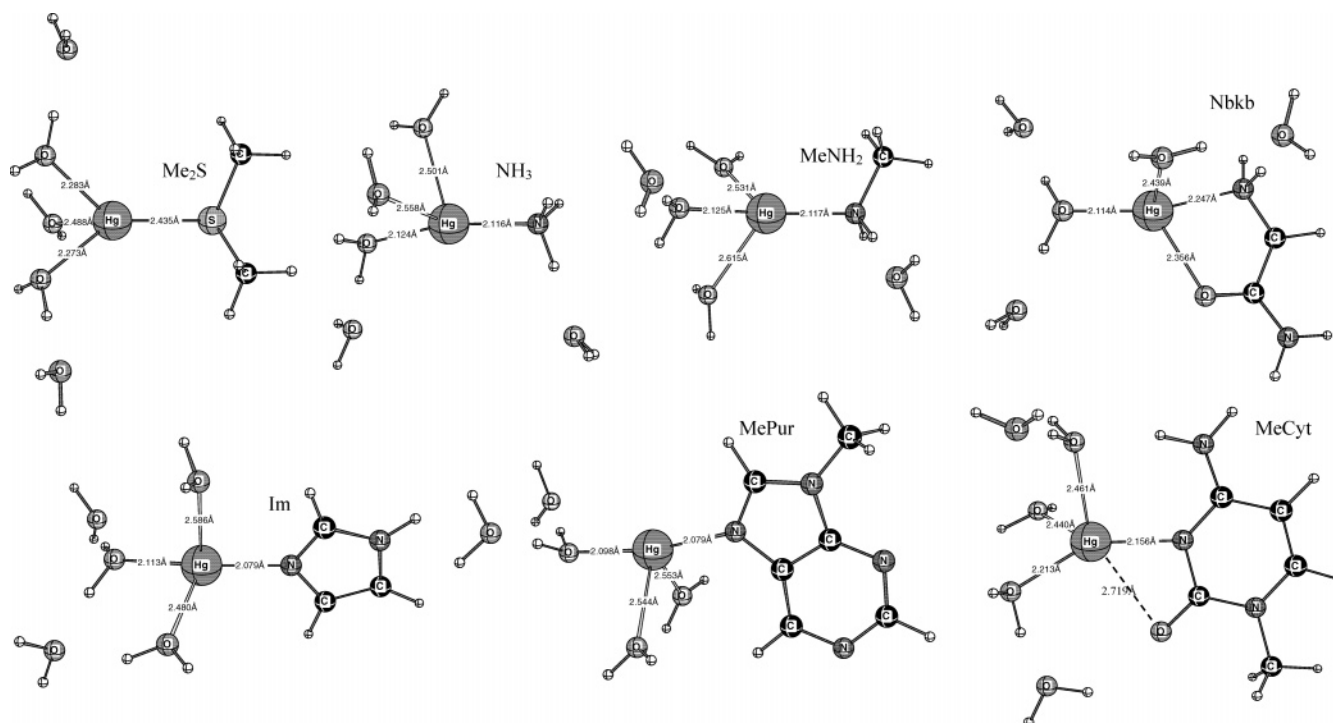
The results in Table 3 rationalize why both “soft” metals, Hg<sup>2+</sup> and MeHg<sup>+</sup>, form stronger bonds with negatively charged ligands containing the “soft” S<sup>-</sup> donor but weaker bonds with neutral ligands containing the “soft” S donor, as compared to the “harder” O<sup>-</sup> or N donor. For the negatively charged ligands, Hg<sup>2+</sup> and MeHg<sup>+</sup> have much more favorable electrostatic and orbital interactions with MeS<sup>-</sup> than with MeCOO<sup>-</sup> or Me<sub>2</sub>PO<sub>4</sub><sup>-</sup>. On the other hand, for the neutral ligands, both mercury species have much more favorable electrostatic interactions with the “hard” NH<sub>3</sub> than with the “softer” SH<sub>2</sub> (by 51 kcal/mol), which outweigh the more favorable orbital interactions with SH<sub>2</sub> than with NH<sub>3</sub> (by 18 kcal/mol).

The ratio of the orbital to the electrostatic contributions,  $\Delta E_{\text{orb}}/\Delta E_{\text{elec}}$ , reveals the relative covalent vs ionic character of the Hg–L bond (Figure 4). Neutral ligands containing a “soft” S donor exhibit more covalent bond character than those with a “harder” N/O donor, as evidenced by a  $\Delta E_{\text{orb}}/\Delta E_{\text{elec}}$  ratio of 1.42 (0.87) for Hg–SH<sub>2</sub> (MeHg–SH<sub>2</sub>) that is significantly greater than the respective ratio of 0.85 (0.60) for Hg–OH<sub>2</sub> (MeHg–OH<sub>2</sub>) or 0.73 (0.54) for Hg–NH<sub>3</sub> (MeHg–NH<sub>3</sub>). The covalent/ionic ratio for Hg<sup>2+</sup> complexed to a neutral ligand is greater than that for MeHg<sup>+</sup>, indicating more covalent bonding with Hg<sup>2+</sup> as compared to MeHg<sup>+</sup>. In contrast to the neutral ligands, the covalent/ionic ratio for Hg<sup>2+</sup> complexed to a negatively charged ligand is similar to that for MeHg<sup>+</sup> (0.37–0.48), indicating a predominantly ionic Hg–L bond for both mercury species.

**Ligand Exchange Free Energies in Various Dielectric Media.** To determine the protein and DNA functional groups that Hg<sup>2+</sup> and MeHg<sup>+</sup> could target in aqueous solution, we evaluated the free energy,  $\Delta G^{80}$ , for replacing one or more

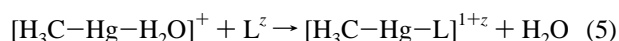
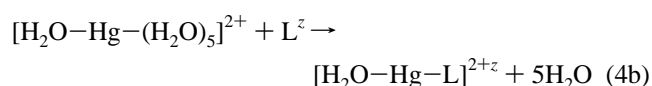
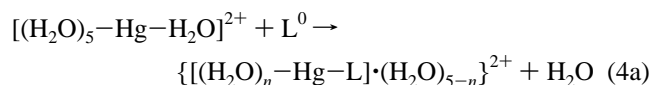


**Figure 4.** Ratio of the orbital to the electrostatic contributions to the Hg–L bond formation energy as a function of ligand type.



**Figure 5.** Fully optimized B3-PW91/Å structures of tetracoordinated inorganic mercury complexes,  $\{[(\text{H}_2\text{O})_n\text{-Hg-L}]\cdot(\text{H}_2\text{O})_{5-n}\}^{2+}$ , with L = Me<sub>2</sub>S, NH<sub>3</sub>, MeNH<sub>2</sub>, Nbbk, Im, MePur, and MeCyt.

metal-bound water molecules with the model ligands in Figure 1



In eq 4a, the symbol “·” separates the first shell from the second shell. Hg<sup>2+</sup> is modeled as an octahedral hydrate, as it is experimentally found to be hexahydrated in aqueous solution.<sup>64</sup> Upon exchanging a metal-bound water molecule for a neutral

nonaqua ligand (eq 4a), Hg<sup>2+</sup> was initially assumed to be hexacoordinated. However, during optimization of the dicationic complexes containing Me<sub>2</sub>S, NH<sub>3</sub>, MeNH<sub>2</sub>, Nbbk, Im, MePur, and MeCyt, Hg<sup>2+</sup> spontaneously became tetracoordinated to these ligands with two or three water molecules in the second shell (Figure 5), while it remained hexacoordinated to the other neutral ligands (MeOH, H<sub>2</sub>S, MeSH, Bkb, MeAde, and MeGua). As the most common coordination number of Hg<sup>2+</sup> in the CSD is two,<sup>65,66</sup> linear Hg<sup>2+</sup> and MeHg<sup>+</sup> complexes (see structures in Table 1) were also fully optimized. On the basis of the B3-PW91/Å fully optimized geometries of the metal complexes, the ΔG<sup>80</sup> for eqs 4a, 4b, and 5 were computed using eqs 1 and 2 (Table 4). Note that the available experimental ΔG<sup>80</sup> values are close to the respective computed values (Table 4).

The results in Table 4 show that eq 4a is more favorable than eq 4b in the gas phase, mainly because the energy needed



**TABLE 4: Calculated Water (W) → Ligand (L) Exchange Free Energies (kcal/mol) in Aqueous Solution<sup>a</sup>**

L <sup>z</sup>	[W <sub>5</sub> -Hg-W] <sup>2+</sup> + L <sup>z</sup> → [W <sub>n</sub> -Hg-L]·W <sub>5-n</sub> <sup>2+z</sup> + W		[W-Hg-W <sub>5</sub> ] <sup>2+</sup> + L <sup>z</sup> → [W-Hg-L] <sup>2+z</sup> + 5W		[H <sub>3</sub> C-Hg-W] <sup>+</sup> + L <sup>z</sup> → [H <sub>3</sub> C-Hg-L] <sup>1+z</sup> + W	
	ΔG <sup>1</sup>	ΔG <sup>80</sup>	ΔG <sup>1</sup>	ΔG <sup>80</sup>	ΔG <sup>1</sup>	ΔG <sup>80</sup>
MeOH	-1.8 <sup>b</sup>	13.0 <sup>b</sup>	69.0	21.9	-4.6	1.5
H <sub>2</sub> S	-3.7 <sup>b</sup>	3.7 <sup>b</sup>	59.3	3.4	-2.5	0.2
MeSH	-18.7 <sup>b</sup>	-3.9 <sup>b</sup>	41.2	0.7	-9.0	-1.4
Me <sub>2</sub> S	-26.3 <sup>c</sup>	-3.7 <sup>c</sup>	27.0	-3.1	-14.5	-2.2
NH <sub>3</sub>	-23.0 <sup>c</sup>	-14.3 <sup>c</sup>	44.4	-12.7	-18.7	-10.7
						(-10.4)
MeNH <sub>2</sub>	-26.4 <sup>c</sup>	-12.4 <sup>c</sup>	34.5	-9.9	-20.6	-8.0
		(-11.8)				(-10.3)
Nbkb	-45.3 <sup>d</sup>	-12.5 <sup>d</sup>	3.1	-10.4	-27.0	-10.6
Bkb	-21.4 <sup>b</sup>	12.4 <sup>b</sup>	30.4	16.0	-20.0	1.6
Im	-40.1 <sup>c</sup>	-10.5 <sup>c</sup>	14.7	-4.7	-26.8	-10.2
MePur	-30.6 <sup>c</sup>	0.5 <sup>c</sup>	21.9	10.6	-17.3	3.8
	-7.2 <sup>e</sup>	5.7 <sup>e</sup>				
MeAde	-30.5 <sup>b</sup>	-1.6 <sup>b</sup>	13.2	14.5	-15.8	4.4
MeGua	-48.6 <sup>b</sup>	7.7 <sup>b</sup>	-14.7	5.6	-33.2	-2.5
MeCyt	-47.8 <sup>c</sup>	2.1 <sup>c</sup>	-4.8	2.4	-30.5	-3.1
MeThy <sup>-</sup>			-194.4	-17.2	-135.3	-14.3
DMP <sup>-</sup>	-195.7 <sup>c</sup>	4.9 <sup>c</sup>	-166.9	3.1	-120.0	-2.2
Ace <sup>-</sup>			-185.7	-6.0	-136.6	-5.7
				(-8.0)		(-4.3)
MeS <sup>-</sup>			-222.6	-38.4	-156.2	-19.7
Cl <sup>-</sup>			-182.5	-9.0	-140.1	-6.0
				(-9.2)		(-7.1)

<sup>a</sup> Computed using eqs 1 and 2 based on B3-PW91/A fully optimized geometries; numbers in brackets are available experimental values. <sup>b</sup>  $n = 5$ ; i.e., [(H<sub>2</sub>O)<sub>5</sub>-Hg-L]<sup>2+</sup>. <sup>c</sup>  $n = 3$ ; i.e., [(H<sub>2</sub>O)<sub>3</sub>-Hg-L]·(H<sub>2</sub>O)<sub>2</sub><sup>2+</sup>. <sup>d</sup>  $n = 2$ ; i.e., [(H<sub>2</sub>O)<sub>2</sub>-Hg-Nbkb]·(H<sub>2</sub>O)<sub>3</sub><sup>2+</sup> (Figure 5). <sup>e</sup> Free energy for [(H<sub>2</sub>O)<sub>5</sub>-Hg-H<sub>2</sub>O]<sup>2+</sup> + MePur → [(H<sub>2</sub>O)<sub>3</sub>-Hg-MePur]<sup>2+</sup> + 3(H<sub>2</sub>O).

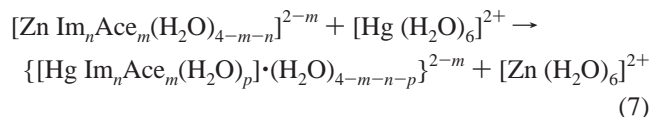
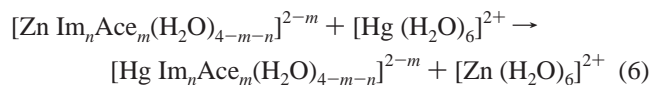
to break extra Hg-H<sub>2</sub>O bonds in forming a linear complex exceeds the entropy gain in the water released (ΔG<sup>1</sup> for eq 4a is more negative than that for eq 4b). However, solvent effects generally disfavor the water → ligand exchange for eqs 4a and 4b involving ligands that are bulky or negatively charged. The latter is because the substituted Hg complex is bulkier or has one less net positive charge than the Hg<sup>2+</sup> hexahydrate, and is thus more poorly solvated. On the other hand, solvent effects generally favor the exchange of five water molecules for a small neutral ligand in eq 4b because of the solvation free energy gain of the linear [H<sub>2</sub>O-Hg-L]<sup>2+</sup> complex relative to the bulkier, hexahydrated Hg<sup>2+</sup> and/or the entropic gain in releasing five water molecules. Consequently, in interpreting the results below, we focus on the more favorable ΔG<sup>80</sup> of the two reactions, eqs 4a and 4b.

The ligand exchange free energies in Table 4 show that the backbone carbonyl oxygen is predicted to bind monodentately to both Hg<sup>2+</sup> and MeHg<sup>+</sup> in solvent-inaccessible cavities (negative ΔG<sup>ε</sup>, ε ≪ 1, for Bkb). As expected, deprotonated Cys is the preferred target for both Hg<sup>2+</sup> and MeHg<sup>+</sup>, as the most negative ΔG<sup>1</sup> and ΔG<sup>80</sup> correspond to MeS<sup>-</sup>. Contrary to HSAB expectations however, neutral N-containing ligands are more likely to interact with Hg<sup>2+</sup> and MeHg<sup>+</sup> than the S-containing counterparts: the ΔG<sup>1</sup> and ΔG<sup>80</sup> for forming NH<sub>3</sub> and MeNH<sub>2</sub> complexes are more favorable than those for forming SH<sub>2</sub> and MeSH complexes, respectively.

In addition to the protein ligands, MeGua, MeCyt, and DMP<sup>-</sup> may form linear complexes with MeHg<sup>+</sup> in aqueous solution (Table 4, negative ΔG<sup>80</sup>). As for the other two DNA bases, we cannot conclude if MeAde could interact with Hg<sup>2+</sup> because the ΔG<sup>80</sup> for eq 4a (-1.6 kcal/mol) is within the error limits of the present calculations (Table 4), while thymine is neutral at physiological pH and cannot interact with Hg<sup>2+</sup> or MeHg<sup>+</sup>, unless it were deprotonated at N3 (Table 4, negative ΔG<sup>ε</sup>, ε ≥ 1 for MeThy<sup>-</sup>).

**Zn<sup>2+</sup> → Hg<sup>2+</sup> Exchange Free Energies in Model “Catalytic” Zn-Binding Sites.** We chose to study the Zn<sup>2+</sup> → Hg<sup>2+</sup>

exchange in “catalytic” as opposed to “structural” Zn sites, because negatively charged Cys, the most preferred inner-shell ligand for “structural” Zn, is known to have higher affinity for Hg<sup>2+</sup> than zinc.<sup>35</sup> In contrast to “structural” Zn sites, His, Asp/Glu, and water molecules are found to be the most preferred inner-shell ligands for Zn<sup>2+</sup> in “catalytic” Zn sites.<sup>67</sup> Assuming that Hg<sup>2+</sup> has found a “catalytic” Zn-binding site (characterized by a dielectric constant ε), we assessed if it could replace Zn<sup>2+</sup> by computing the Zn<sup>2+</sup> → Hg<sup>2+</sup> exchange free energies in rigid and flexible model Zn-binding sites as follows:



In eqs 6 and 7, Im and Ace model His and Asp/Glu side chains, respectively,  $n = 0-2$ ,  $m = 0-3$ , and  $p = 1-3$ . As for Hg<sup>2+</sup>, Zn<sup>2+</sup> is experimentally found to be hexahydrated in aqueous solution.<sup>64</sup> Eq 6 models metal exchange in a rigid Zn<sup>2+</sup>-binding site that forces the incoming Hg<sup>2+</sup> to adopt Zn’s tetrahedral geometry, while eq 7 models metal exchange in a more flexible Zn<sup>2+</sup>-binding site that allows Hg<sup>2+</sup> to adopt its lowest-energy geometry.

The Zn<sup>2+</sup> → Hg<sup>2+</sup> exchange free energies for reactions 6 and 7 in the gas phase and in various dielectric media are summarized in Table 5. Note that, in two of the model “catalytic” Zn<sup>2+</sup>-binding sites studied (Table 5, reactions 3 and 4), we could not locate a stable Hg-substituted tetrahedral complex, which spontaneously converted to a linear or trigonal structure during geometry optimization. Interestingly, for each of the tetrahedral complexes in Table 5, charge transfer from the ligands to Hg<sup>2+</sup> (0.49–0.62 e) is greater than that to Zn<sup>2+</sup> (0.32–0.41 e), indicating that Hg<sup>2+</sup> can accept more negative



**TABLE 5: Enthalpies ( $\Delta H^1$ ) and Free Energies ( $\Delta G^\epsilon$ ) for  $\text{Zn}^{2+} \rightarrow \text{Hg}^{2+}$  Exchange in Model “Catalytic” Zn-Binding Sites of Varying Dielectric Constant  $\epsilon$  (in kcal/mol)<sup>a</sup>**

no.	reactant + $[\text{HgW}_6]^{2+}$	product + $[\text{ZnW}_6]^{2+}$	$\text{CN}_{\text{Hg}}^b$	$\text{CT}_{\text{Zn}}^c$	$\text{CT}_{\text{Hg}}^d$	$\Delta H^1$	$\Delta G^1$	$\Delta G^4$	$\Delta G^{20}$	$\Delta G^{80}$
1	$[\text{Zn Im W}_3]^{2+}$	$[\text{Hg Im W}_3]^{2+}$ $([\text{Hg Im W}] \cdot \text{W}_2)^{2+}$	4 2	0.32	0.49 0.61	-12.8 -16.3	-7.3 -10.4	-8.7 -8.2	-8.8 -7.9	-8.8 -7.7
2	$[\text{Zn Im}_2 \text{W}_2]^{2+}$	$[\text{Hg Im}_2 \text{W}_2]^{2+}$ $([\text{Hg Im}_2] \cdot \text{W}_2)^{2+}$	4 2	0.36	0.58 0.68	-19.6 -22.8	-16.1 -18.7	-18.5 -18.0	-18.8 -18.7	-18.8 -18.7
3 <sup>e</sup>	$[\text{Zn Ace W}_3]^+$	$([\text{Hg Ace W}] \cdot \text{W}_2)^+$	2	0.35	0.67	-13.1	-10.5	-11.9	-11.9	-11.8
4 <sup>e</sup>	$[\text{Zn Im Ace W}_2]^+$	$([\text{Hg Im Ace W}] \cdot \text{W})^+$	3	0.31	0.66	-15.0	-11.5	-13.4	-13.4	-13.2
5	$[\text{Zn Im}_2 \text{Ace W}]^+$	$[\text{Hg Im}_2 \text{Ace W}]^+$ $([\text{Hg Im}_2 \text{Ace}] \cdot \text{W})^+$	4 3	0.40	0.56 0.61	-7.3 -7.3	-3.7 -5.3	-11.2 -13.9	-13.5 -16.7	-13.9 -17.1
6	$[\text{Zn Ace}_2 \text{W}_2]^0$	$[\text{Hg Ace}_2 \text{W}_2]^0$ $([\text{Hg Ace}_2 \text{W}] \cdot \text{W})^0$	4 3	0.35	0.62 0.66	-8.0 -3.0	-3.6 -1.0	-8.4 -9.8	-8.5 -11.7	-8.6 -12.0
7	$[\text{Zn Im Ace}_2 \text{W}]^0$	$[\text{Hg Im Ace}_2 \text{W}]^0$ $([\text{Hg Ace}_2 \text{W}] \cdot \text{Im})^0$	4 3	0.36	0.60 0.66	-4.1 -0.4	-0.4 2.0	-5.1 -3.0	-6.4 -4.2	-6.7 -4.3
8	$[\text{Zn Ace}_3 \text{W}]^-$	$[\text{Hg Ace}_3 \text{W}]^-$	4	0.41	0.57	-6.6	-3.0	-9.2	-10.5	-10.8

<sup>a</sup> Im = imidazole, W = H<sub>2</sub>O, Ace = CH<sub>3</sub>COO<sup>-</sup>. <sup>b</sup> Coordination number of Hg. <sup>c</sup> Net NBO charge transferred by the ligands to Zn<sup>2+</sup>. <sup>d</sup> Net NBO charge transferred by the ligands to Hg<sup>2+</sup>. <sup>e</sup> A stable tetrahedral Hg-substituted complex could not be found.

charge from the ligands than Zn<sup>2+</sup>. Correspondingly, the gas-phase Zn<sup>2+</sup> → Hg<sup>2+</sup> exchange enthalpies,  $\Delta H^1$ , are negative. In contrast, the gas-phase entropy term,  $\Delta H^1 - \Delta G^1$ , disfavors Zn<sup>2+</sup> → Hg<sup>2+</sup> exchange and may contribute significantly to the free energy (e.g., Table 5, second last reaction); thus, it should not be neglected in computing  $\Delta G^1$ . All the  $\Delta G^\epsilon$ ,  $\epsilon \geq 4$ , in Table 5 are negative, indicating that Hg<sup>2+</sup> can displace Zn<sup>2+</sup> regardless of the solvent accessibility and the relative rigidity/flexibility of the Zn-binding site.

## Discussion

**Interaction Differences Between Hg<sup>2+</sup> and MeHg<sup>+</sup>.** The key factor governing the differences between inorganic Hg<sup>2+</sup> and organic MeHg<sup>+</sup> in their interactions with different ligands lies in the charge difference on the two metals. Because Hg<sup>2+</sup> has greater positive charge than MeHg<sup>+</sup>, it forms less linear structures, as well as shorter and thus stronger Hg–L bonds (Table 2). The finding herein that organic mercury compounds have less stable complexation energies than the inorganic counterparts is in accord with the observed kinetic lability of the MeHg<sup>+</sup> cation.<sup>1</sup> Although both mercury species form a predominantly ionic Hg–L bond with a negatively charged ligand, Hg<sup>2+</sup> forms a less-ionic bond with a neutral ligand, as compared to MeHg<sup>+</sup> (Figure 4).

**Negatively Charged Ligands Obey HSAB Principle; Neutral Ligands May Not.** In accord with the HSAB principle, the “soft” Hg<sup>2+</sup> and MeHg<sup>+</sup> centers prefer negatively charged ligands containing the “soft” S<sup>-</sup> donor rather than the “harder” O<sup>-</sup>/N<sup>-</sup> donor in the gas phase and in aqueous solution (Table 4). However, contrary to the HSAB principle, Hg<sup>2+</sup> and MeHg<sup>+</sup> prefer neutral ligands containing the “harder” N donor rather than the “soft” S donor (Table 4), partly because both mercury species have more favorable electrostatic interactions with the former than with the latter (Table 3).

**Hg<sup>2+</sup> and MeHg<sup>+</sup> Biological Targets.** The finding here that solvent-inaccessible backbone carbonyl oxygen atoms could bind monodentately to both Hg<sup>2+</sup> and MeHg<sup>+</sup> suggests that these two mercury species could potentially target any protein. The deprotonated Cys side chain, modeled by MeS<sup>-</sup>, is the preferred biological target of both Hg<sup>2+</sup> and MeHg<sup>+</sup>. In addition to the “soft” Cys(S<sup>-</sup>) and Met(S) atoms, ligands containing the “harder” O<sup>-</sup>/N donor such as deprotonated Asp/Glu (Ace<sup>-</sup>), His (Im), and Lys (MeNH<sub>2</sub>) side chains could also interact with both mercury species (Table 4). These protein targets are consistent with the observation that deprotonated Cys, Met, Asp/Glu, His, and Lys side chains are bound to Hg<sup>2+</sup> in the PDB structures<sup>65</sup> (Table 1 in Supporting Information).

Neutral Gua and Cyt DNA bases are predicted to interact with MeHg<sup>+</sup> in aqueous solution. The negative  $\Delta G^{80}$  for formation of [Me–Hg–MeGua]<sup>+</sup> in Table 4 is consistent with the experimentally observed formation of [Me–Hg–Gua]<sup>+</sup> in aqueous solution.<sup>7</sup> Since C<sup>2</sup>–O, N<sup>1</sup>–H, and N<sup>4</sup>–H of Cyt hydrogen bond to N<sup>2</sup>–H, N<sup>1</sup>–H, and C<sup>6</sup>–O of Gua, respectively (see Figure 1b), in forming a Watson–Crick base pair, N<sup>3</sup> coordination of Cyt to MeHg<sup>+</sup> would disrupt Cyt–Gua base pairing.

**Hg<sup>2+</sup> Can Compete with Zn<sup>2+</sup> for Non-Cysteine Residues in “Catalytic” Zn Sites.** If Hg<sup>2+</sup> could find a “catalytic” Zn-binding site, then Hg<sup>2+</sup> can replace Zn<sup>2+</sup>, as evidenced by the negative metal exchange free energies in Table 5. This is consistent with experimental findings that Hg<sup>2+</sup> can replace biological Zn<sup>2+</sup> in certain Zn enzymes such as carboxypeptidase A (Table 1 in Supporting Information). The thermodynamical preference of the harder N and O<sup>-</sup>-containing side chains for the “soft” Hg rather than the “borderline” Zn is probably due to relativistic effects resulting in a strong stabilization of mercury’s vacant 6s orbitals, which in turn enhances its electron-accepting ability. Consequently, charge transfer from a given set of ligands to Hg<sup>2+</sup> is greater than that to Zn<sup>2+</sup>, thereby allowing Hg<sup>2+</sup> to compete for the Zn<sup>2+</sup> ligands (Table 5). Studies on metal–ligand interactions involving the group 11 monocations have also found the bond energies of Au(I) to be greater than those of Ag(I) because of the relativistic stabilization of gold’s vacant 6s orbitals, which enhances its electron-accepting ability and thus its interactions with ligands, as compared with Ag(I).<sup>68</sup>

In certain rigid Zn-binding sites (Table 5, reactions 1, 2, 5–8), Hg<sup>2+</sup>, which has a larger ionic radius than Zn<sup>2+</sup> ( $r_{\text{Hg}}/r_{\text{Zn}} = 1.02/0.75$ ), could retain the tetrahedral Zn-binding site geometry, but it attenuates the native metal–ligand bond distances so that the protein might not maintain the proper conformation for its biological function. In the tetrahedral metal complexes in Table 5, the average “native” Zn–N(Im) ( $1.99 \pm 0.04$  Å), Zn–O(Ace<sup>-</sup>) ( $1.97 \pm 0.08$  Å), and Zn–O(water) ( $2.08 \pm 0.06$  Å) distances are shorter than the respective Hg–N(Im) ( $2.19 \pm 0.14$  Å), Hg–O(Ace<sup>-</sup>) ( $2.21 \pm 0.13$  Å), and Hg–O(water) ( $2.54 \pm 0.12$  Å) distances by 0.20, 0.24, and 0.46 Å, respectively. These findings are consistent with the X-ray structures of the native Zn-binding site (PDB ID: 2CTC) and the Hg-substituted binding site (PDB ID: 1ARM) in carboxypeptidase A: the average Zn–N(His) and Zn–O(Asp) distances are also shorter than the Hg–N(His) and Hg–O(Asp) distances by 0.13 and 0.26 Å, respectively. On the other hand, for flexible binding sites, Hg<sup>2+</sup> may destroy the tetrahedral Zn-binding site geometry by adopting a linear or trigonal geometry (Table 5).

**Biological Implications.** The calculations support several possible mechanisms for Hg poisoning in living cells. By binding to negatively charged/polar amino acid side chains or the protein backbone,  $\text{Hg}^{2+}$  and  $\text{MeHg}^+$  could (1) inactivate essential residues in various proteins/enzymes, (2) deplete certain amino acids that are precursors of neurotransmitters, and (3) disrupt the active conformation structure and thus function of essential proteins. In particular,  $\text{Hg}^{2+}$  could displace the native  $\text{Zn}^{2+}$  cofactor from both structural and catalytic Zn sites, because  $\text{Hg}^{2+}$  can accept more charge from the Zn ligands than  $\text{Zn}^{2+}$  (see above and Table 5). In replacing  $\text{Zn}^{2+}$ ,  $\text{Hg}^{2+}$  may destroy the native tetrahedral binding-site geometry by adopting a linear or trigonal geometry, thus deactivating certain Zn proteins whose tetrahedral Zn-binding sites play an essential role in stabilizing the active protein conformation. In cases where  $\text{Hg}^{2+}$  retains the native tetrahedral binding-site geometry, it could still inhibit the function of Zn enzymes such as carbonic anhydrase.<sup>69–71</sup> Because  $\text{Hg}^{2+}$  is a far better electron acceptor than  $\text{Zn}^{2+}$ , it could accept more charge from a metal-bound hydroxide than the native  $\text{Zn}^{2+}$  cofactor, thus preventing the metal-bound water from acting as a nucleophile in the reaction. In addition, by binding to Gua and Cyt bases and the RNA/DNA phosphate backbone,  $\text{MeHg}^+$  could disrupt Gua-Cyt base pairing and perturb interactions with essential DNA/RNA-binding proteins (Table 4).

The calculations also suggest ways mercury poisoning could be prevented in living cells. Because  $\text{Hg}^{2+}$  can replace  $\text{Zn}^{2+}$  in both “structural” and “catalytic” Zn sites (see above and Table 5), the protein ligands lining the Zn-binding site do not seem to govern selectivity of  $\text{Zn}^{2+}$  over  $\text{Hg}^{2+}$ . The rest of the Zn protein may play a role in choosing  $\text{Zn}^{2+}$  instead of  $\text{Hg}^{2+}$  and other non-native metal cofactors by inducing kinetic barriers or traps that could inhibit an alien metal to enter the native metal-binding site.<sup>72</sup> Under conditions or in proteins that allow  $\text{Hg}^{2+}$  to enter the native metal-binding site, the cell machinery could help to prevent mercury poisoning by using Cys-rich proteins to either regulate the concentrations of mercury and zinc<sup>40</sup> or to abstract the toxic metal from the damaged Zn-binding site and deliver the essential natural cofactor (Zn) to the same site.<sup>73</sup>

**Acknowledgment.** We are grateful to Dr. D. Deubel for assistance in the energy decomposition analyses. We thank Dr. T. Dudev and Ms. Y. Lin for helpful discussions. This work is supported by the National Science Council, Taiwan (NSC contract no. 92-2113-M-001-032), the Institute of Biomedical Sciences, Academia Sinica, and the National Center for High-Performance Computing, Taiwan.

**Supporting Information Available:** Six tables of supporting data. This material is available free of charge via the Internet at <http://pubs.acs.org>.

## References and Notes

- Richens, D. T. *The Chemistry of Aqua Ions*; John Wiley & Sons: New York, 1997.
- Klaassen, C. D. *Casarett and Doull's Toxicology*, International Press ed.; McGraw-Hill: New York, 1996.
- Albers, R.; Pijl, A.; Seinen, W.; Pieters, R.; Bloksma, N. *Immunology* **1996**, *89*, 468–473.
- Jin, G.; Inoue, S.; Urano, T.; Cho, S.; Ouchi, Y.; Cyong, J. *Toxicol. Appl. Pharmacol.* **2002**, *185*, 98–110.
- Hess, E. V. *Toxicology* **2002**, *181*, 65–70.
- Prizant, L.; Olivier, M. J.; Rivest, R.; Beauchamp, A. L. *Can. J. Chem.* **1981**, *59*, 1311–1317.
- Buncel, E.; Norris, A. R.; Racz, W. J.; Taylor, S. E. *Inorg. Chem.* **1981**, *20*, 98–103.
- Norris, A. R.; Kumar, R.; Buncel, E. *J. Inorg. Biochem.* **1984**, *22*, 11.
- Lippard, S. J.; Berg, J. M. *Principles of Bioinorganic Chemistry*; University Science Books: Mill Valley, California, 1994.
- Vallee, B. L.; Ulmer, D. D. *Annu. Rev. Biochem.* **1972**, *41*, 91–128.
- Miller, O. M.; Lund, B. O.; Woods, J. S. *J. Biochem. Toxicol.* **1991**, *6*, 293–298.
- Interactions between glutathione and mercury in the kidney, liver, and blood*; Zalups, R. K., Lash, L. H., Eds.; CRC Press: Boca Raton, 1996; pp 145–163.
- Benov, L. C.; Benchev, I. C.; Monovich, O. H. *Chem.-Biol. Interact.* **1990**, *76*, 321–332.
- Hamer, D. H. *Annu. Rev. Biochem.* **1986**, *55*, 913–951.
- Predki, P. F.; Sarkar, B. *J. Biol. Chem.* **1992**, *267*, 5842–5846.
- Hartwig, A. *Antiox. Redox Signaling* **2001**, *3*, 625–634.
- Hartwig, A.; Asmuss, M.; Blessing, H.; Hoffmann, S.; Jahnke, G.; Khandelwal, S.; Polzer, A.; Burkle, A. *Food Chem. Toxicol.* **2002**, *40*, 1179–1184.
- Asmuss, M.; Mullenders, L. H. F.; Hartwig, A. *Toxicol. Lett.* **2000**, *112–113*, 227–231.
- Razmiafshari, M.; Kao, J.; d'Avignon, A.; Zawia, N. H. *Toxicol. Appl. Pharmacol.* **2001**, *172*, 1–10.
- Craig, P. J.; Wilkinson, G. *Comprehensive Organometallic Chemistry*; Pergamon: New York, 1982.
- Goggin, P. L.; Woodward, L. A. *Trans. Faraday Soc.* **1962**, *58*, 1495.
- Erni, I. W.; Geier, G. *Helv. Chim. Acta* **1979**, *62*, 1007–1015.
- Raycheba, J. M. T.; Geier, G. *Inorg. Chem.* **1979**, *18*, 2486–2491.
- Libich, S.; Rabenstein, D. L. *Anal. Chem.* **1973**, *45*, 118–124.
- Sudmeier, J. L.; Perkins, T. G. *J. Magn. Reson.* **1978**, *30*, 491.
- Geier, G.; Gross, H. *Inorg. Chim. Acta* **1989**, *156*, 91.
- Tamura, K.; Yasunaga, T. *Bull. Chem. Soc. Jpn.* **1978**, *51*, 2928.
- Barone, V.; Bencini, A.; Uytterhoeven, M. G. *J. Phys. Chem.* **1995**, *99*, 12743–12750.
- Barone, V.; Bencini, A.; Totti, F.; Uytterhoeven, M. G. *Organometallics* **1996**, *15*, 1465–1469.
- Cundari, T. R.; Yoshikawa, A. *J. Comput. Chem.* **1998**, *19*, 902–911.
- Tossell, J. A. *J. Phys. Chem. A* **1998**, *102*, 3587–3591.
- Buncel, E.; Hunter, B. K.; Kumar, R.; Norris, A. R. *J. Inorg. Biochem.* **1984**, *20*, 171–181.
- Sheldrick, W. S.; Heeb, G. *Inorg. Chim. Acta* **1992**, *194*, 67–73.
- Yamamura, T.; Watanabe, T.; Kikuchi, A.; Yamane, T.; Ushiyama, M.; Hirota, H. *Inorg. Chem.* **1997**, *36*, 4849–4859.
- Rulisek, L.; Havlas, Z. *J. Am. Chem. Soc.* **2000**, *122*, 10428–10439.
- Tossell, J. A. *J. Phys. Chem. A* **2001**, *105*, 935.
- Rulisek, L.; Havlas, Z. *J. Phys. Chem. A* **2002**, *106*, 3855–3866.
- Matzapetakis, M.; Farrer, B. T.; Weng, T.-C.; Hemmingsen, L.; Penner-Hahn, J. E.; Pecoraro, V. L. *J. Am. Chem. Soc.* **2002**, *124*, 8042–8054.
- DeSilva, T. M.; Veglia, G.; Porcelli, F.; Prantner, A. M.; Opella, S. J. *Biopolymers* **2002**, *64*, 189–197.
- Dudev, T.; Lim, C. *Chem. Rev.* **2003**, *103*, 773–787.
- Bernstein, F. C.; Koetzle, T. F.; Williams, G. J. B.; Meyer, E. F.; Brice, M. D.; Rodgers, J. R.; Kennard, O.; Shimanouchi, T.; Tasumi, M. *J. Mol. Biol.* **1977**, *122*, 535–542.
- Frisch, M. J.; Trucks, G. W.; Schlegel, H. B.; Scuseria, G. E.; Robb, M. A.; Cheeseman, J. R.; Montgomery, J. A., Jr.; Vreven, T.; Kudin, K. N.; Burant, J. C.; Millam, J. M.; Iyengar, S. S.; Tomasi, J.; Barone, V.; Mennucci, B.; Cossi, M.; Scalmani, G.; Rega, N.; Peterson, G. A.; Nakatsuji, H.; Hada, M.; Ehara, M.; Toyota, K.; Fukuda, R.; Hasegawa, J.; Ishida, M.; Nakajima, T.; Honda, Y.; Kitao, O.; Nakai, H.; Klene, M.; Li, X.; Knox, J. E.; Hratchian, H. P.; Cross, J. B.; Adamo, C.; Jaramillo, J.; Gomperts, R.; Stratmann, R. E.; Yazyev, O.; Austin, A. J.; Cammi, R.; Pomelli, C.; Ochterski, J. W.; Ayala, P. Y.; Morokuma, K.; Voth, G. A.; Salvador, P.; Dannenberg, J. J.; Zakrzewski, V. G.; Dapprich, S.; Daniels, A. D.; Strain, M. C.; Farkas, O.; Malick, D. K.; Rabuck, A. D.; Raghavachari, K.; Foresman, J. B.; Ortiz, J. V.; Cui, Q.; Baboul, A. G.; Clifford, S.; Cioslowski, J.; Stefanov, B. B.; Liu, G.; Liasehenko, A.; Piskorz, P.; Komaromi, I.; Martin, R. L.; Fox, D. J.; Keith, T.; Al-Laham, M. A.; Peng, C. Y.; Nanayakkara, A.; Challacombe, M.; Gill, P. M. W.; Johnson, B.; Chen, W.; Wong, M. W.; Gonzalez, C.; Pople, J. A. *Gaussian 03*, rev. B.03; Gaussian, Inc.: Pittsburgh, PA, 2003.
- Becke, A. D. *Phys. Rev.* **1988**, *A38*, 3098–3100.
- Perdew, J. P.; Chevary, J. A.; Vosko, S. H.; Jackson, K. A.; Pederson, M. R.; Singh, D. J.; Fiolhais, C. *Phys. Rev. B* **1992**, *46*, 6671.
- Andrae, D.; Häussermann, U.; Dolg, M.; Stoll, H.; Preuss, H. *Theor. Chim. Acta* **1990**, *77*, 123–141.
- Dolg, M.; Wedig, U.; Stoll, H.; Preuss, H. *J. Chem. Phys.* **1987**, *86*, 866–872.

- (47) Hariharan, P. C.; Pople, J. A. *Theor. Chim. Acta* **1973**, *28*, 213–222.
- (48) Clark, T.; Chandrasekhar, J.; Schleyer, P. v. R. *J. Comput. Chem.* **1983**, *4*, 294–301.
- (49) Krishnan, R.; Binkley, J. S.; Seeger, R.; Pople, J. A. *J. Chem. Phys.* **1980**, *72*, 650–654.
- (50) Lee, C.; Yang, W.; Parr, R. G. *Phys. Rev.* **1988**, *B37*, 785–789.
- (51) Ziegler, T.; Rauk, A. *Inorg. Chem.* **1979**, *18*, 1755–1759.
- (52) Frenking, G.; Fröhlich, N. *Chem. Rev.* **2000**, *100*, 717–774.
- (53) Te Velde, G.; Bickelhaupt, F. M.; Baerends, E. J.; Fonseca Guerra, C.; Van Gisbergen, S. J. A.; Snijders, J. G.; Ziegler, T. *J. Comput. Chem.* **2001**, *22*, 931–967.
- (54) Perdew, J. P. *Phys. Rev. B* **1986**, *33*, 8822.
- (55) Snijders, J. G.; Baerends, E. J.; Vernooijs, P. *At. Data Nucl. Data Tables* **1982**, *26*, 483–509.
- (56) Baerends, E. J.; Ellis, D. E.; Ros, P. *Chem. Phys.* **1973**, *2*, 41–51.
- (57) Van Lenthe, E.; Ehlers, A. E.; Baerends, E. J. *J. Chem. Phys.* **1999**, *110*, 8943.
- (58) Deubel, D. V. *J. Am. Chem. Soc.* **2002**, *124*, 5834–5842.
- (59) Scott, A. P.; Radom, L. *J. Phys. Chem.* **1996**, *100*, 16502–16513.
- (60) Marten, B.; Kim, K.; Cortis, C.; Friesner, R. A.; Murphy, R. B.; Ringnalda, M. N.; Sitkoff, D.; Honig, B. *J. Phys. Chem.* **1996**, *100*, 11775–11788.
- (61) Allen, F. H. *Acta Crystallogr.* **2002**, *B58*, 380–388.
- (62) Gordy, W.; Sheridan, J. J. *J. Chem. Phys.* **1954**, *22*, 92.
- (63) Vosko, S. H.; Wilk, L.; Nusair, M. *Can. J. Phys.* **1980**, *58*, 1200–1211.
- (64) Marcus, Y. *Chem. Rev.* **1988**, *88*, 1475–1498.
- (65) Rulisek, L.; Vondrasek, J. *J. Inorg. Biochem.* **1998**, *71*, 115–127.
- (66) Dudev, M.; Wang, J.; Dudev, T.; Lim, C. *Inorg. Chem.*, submitted.
- (67) Dudev, T.; Lin, Y. L.; Dudev, M.; Lim, C. *J. Am. Chem. Soc.* **2003**, *125*, 3168–3180.
- (68) Tai, H.; Krossing, I.; Seth, M.; Deubel, D. V. *Organometallics* **2004**, *23*, 2343–2349.
- (69) Silverman, D. N.; Lindsog, S. *Acc. Chem. Res.* **1988**, *21*, 30–36.
- (70) Christianson, D. W.; Cox, J. D. *Annu. Rev. Biochem.* **1999**, *68*, 33–57.
- (71) Lin, Y.-l.; Lee, Y.-M.; Lim, C. *J. Am. Chem. Soc.* **2005**, *127*, 11336–11347.
- (72) Babu, C. S.; Lim, C. Manuscript in preparation.
- (73) Roesijadi, G. *Cell. Mol. Biol.* **2000**, *46*, 393–404.